Costal Cartilage Graft Repair Osteochondral Defect in a Mouse Model

Yidan Pang[1]*, Yiyang Ma[1]* iD, Kaiwen Zheng[1] iD, Siyuan Zhu[2], Hongyu Sui[3], Hao Ren[3], Kang Liu[4], Wei Li[4], Yigang Huang[1], Dajiang Du[1], Junjie Gao[1,5], and Changqing Zhang[1] iD

Abstract

Objective. Osteochondral defects develop into osteoarthritis without intervention. Costal cartilage can be utilized as an alternative source for repairing osteochondral defect. Our previous clinical study has shown the successful osteochondral repair by costal cartilage graft with integration into host bone bed. In this study, we investigate how cartilaginous graft adapt to osteochondral environment and the mechanism of bone-cartilage interface formation. *Design.* Costal cartilage grafting was performed in C57BL/6J mice and full-thickness osteochondral defect was made as control. 3D optical profiles and micro-CT were applied to evaluate the reconstruction of articular cartilage surface and subchondral bone as well as gait analysis to evaluate articular function. Histological staining was performed at 2, 4, and 8 weeks after surgery. Moreover, costal cartilage from transgenic mice with fluorescent markers were transplanted into wild-type mice to observe the *in vivo* changes of costal chondrocytes. *Results.* At 8 weeks after surgery, 3D optical profiles and micro-CT showed that in the graft group, the articular surface and subchondral bone were well preserved. Gait analysis and International Cartilage Repair Society (ICRS) score evaluation showed a good recovery of joint function and histological repair in the graft group. Safranin O staining showed the gradual integration of graft and host tissue. Costal cartilage from transgenic mice with fluorescent markers showed that donor-derived costal chondrocytes turned into osteocytes in the subchondral area of host femur. *Conclusion.* Costal cartilage grafting shows both functional and histological repair of osteochondral defect in mice. Graft-derived costal chondrocytes differentiate into osteocytes and contribute to endochondral ossification.

Keywords

[1]Department of Orthopaedic Surgery, Shanghai Sixth People's Hospital Affiliated to Shanghai Jiao Tong University School of Medicine, Shanghai, China
[2]Department of General Surgery, Shanghai Sixth People's Hospital Affiliated to Shanghai Jiao Tong University School of Medicine, Shanghai, China
[3]School of Information Science and Technology, ShanghaiTech University, Shanghai, China
[4]Beixcell (Beijing) Biotechnology Ltd, Beijing, China
[5]Jinjiang Municipal Hospital (Shanghai Sixth People's Hospital Fujian), Jinjiang City, Quanzhou, China

*These authors contributed equally.

Corresponding Authors:
Yigang Huang, Department of Orthopaedic Surgery, Shanghai Sixth People's Hospital Affiliated to Shanghai Jiao Tong University School of Medicine, No. 600, Yishan Road, Shanghai 200233, China.
Email: yiganghuang@sjtu.edu.cn

Dajiang Du, Department of Orthopaedic Surgery, Shanghai Sixth People's Hospital Affiliated to Shanghai Jiao Tong University School of Medicine, No. 600, Yishan Road, Shanghai 200233, China.
Email: dudajiang@sjtu.edu.cn

Junjie Gao, Department of Orthopaedic Surgery, Shanghai Sixth People's Hospital Affiliated to Shanghai Jiao Tong University School of Medicine, No. 600, Yishan Road, Shanghai 200233, China.
Email: colingjj@163.com

Changqing Zhang, Department of Orthopaedic Surgery, Shanghai Sixth People's Hospital Affiliated to Shanghai Jiao Tong University School of Medicine, No. 600, Yishan Road, Shanghai 200233, China.
Email: zhangcq@sjtu.edu.cn

Introduction

Articular cartilage covers and integrates to subchondral bone at the joint surface to reduce friction and to transfer load. Because of its avascular nature, articular cartilage has limited self-repair ability after injury.[1,2] Osteochondral defect may cause cartilage degeneration and develop into osteoarthritis without intervention, which will lead to pain and disability and require a joint replacement at late stage.[3,4] Many clinical methods have been developed to restore osteochondral defect, such as microfracture, osteochondral autograft transplantation, and cartilage tissue engineering.[5] Fibrocartilage forming, donor-site morbidity, limited cell source, and cost-effectiveness have been major barriers to their clinical use.[6,7] Another major concern for all those autologous and tissue-engineered grafts is how they can maintain hyaline cartilage nature while integrate into host tissue to form a transition to subchondral bone, since the stability of osteochondral graft is vital for load bearing.[8]

Costal cartilage is the most abundant source of hyaline cartilage in human body, which has similar composition to articular cartilage.[9] Studies have explored costal cartilage as alternative source for cartilage repair.[10,11] In tissue engineering, costal chondrocytes have higher cell yield and proliferate faster than articular chondrocytes *in vitro* and they can be induced into articular cartilage phenotype under appropriate condition.[11,12] Our previous clinical study of autologous costal cartilage grafting (ACCG) for osteochondral defect showed that ACCG improved hip function and quality of life in young patients within 3-year follow-up.[13] This promising long-term outcome may be due to the good integration between the recipient and the implanted costal cartilage graft, which was shown in delayed gadolinium-enhanced magnetic resonance imaging (dGEMRIC) of patients' femoral head.[13] One of the most important characteristics that distinguishes costal cartilage from articular cartilage is that the human costal cartilage develops into highly hypertrophic type during puberty, and ossification of costal cartilage is arrested when reaching this highly hypertrophy status.[14] Moreover, at the end of puberty, the endochondral ossification of costal cartilage starts, takes place slowly, and lasts throughout whole lifespan,[15,16] which might made ossification more inducible in costal cartilage by external environment.

Our study designs a clinically relevant costal cartilage graft surgery in mice model. We test its effect to repair osteochondral defect and explored the underlying mechanism of the formation of graft-host interface. We provide evidence that costal cartilage graft surgery form steady graft-host interface. Moreover, we traced down long-term transition of costal chondrocytes and observed that costal chondrocytes differentiate into osteocytes during osteochondral repair in the environment of subchondral area but not articular cartilage.

Methods

Experimental Overview

In this experiment, a total of fifty-seven 8-week-old adult male C57BL/6J mice were used based on the published protocol.[17-23] 8-week-old C57BL/6J mice is considered adult.[21,24] In our study, we used osteochondral defect mice model in trochlear groove, trochlear groove of 8-week-old mice is mature and of adequate size.[18]

The costal cartilage graft was either from male C57BL/6J mice of same age or B6/J mGmT mice. Five wild-type mice and 1 transgenic fluorescent mouse were sacrificed at surgery as resource of transplanted costal cartilage. Mice that received surgery were divided into 3 experimental groups (sham, defect, and graft) and sacrificed at 3 time point (2 weeks, 4 weeks, and 8 weeks after surgery). Five mice were used for each experimental group of 2 weeks and 4 weeks, 7 mice for sham group of 8 weeks, 7 mice for defect group of 8 weeks, and 9 mice for graft group of 8 weeks. For recipient of costal cartilage from transgenic mice with fluorescent markers, another 3 mice were used and sacrificed at 8 weeks. 2 weeks, 4 weeks and 8 weeks after surgery, specimens were collected. 8 weeks after surgery, gait analysis was performed on the animals. A postsurgery period of 8 weeks was chosen based on previous publications.[19-23,25,26]

Animals and Animal Procedures

C57BL/6J mice and B6/J mGmT mice were purchased from GemPharmatech Co., Ltd. All animal experiments were conducted according to the regulations and with approval of the Animal Care and Use Committee of Shanghai Sixth People's Hospital (DWSY2021-0938). The animals were housed 3 per cage in the animal experimentation facility under a normal 12-hour light-dark cycle with free access to food and water.

Mouse Model of Osteochondral Defect and Costal Cartilage Graft

The mouse model of osteochondral defect was adapted from previous described ones.[17,20,27] Eight-week-old male C57BL/6J mice were anesthetized with sodium pentobarbital (1% wt/vol) intraperitoneally injected. The right knees were shaved and disinfected with 70% ethanol. The skin was cut with fine scissors and separated from the underlying tissue by blunt dissection. Medial para-patellar arthrotomy was made and the articular surface of distal femur was exposed by placing the knees at flexion position. The incisions of mice in sham group were sewed up layers by layers. For mice in defect group, a full-depth osteochondral defect (0.5 mm in diameter and 2 mm in depth) was made by a G25 needle at the middle of patellar groove. The

syringe needle was placed vertical to the articular surface and then was gently rotated and advanced until its bevel was hidden into the cartilage surface. Then normal saline was used to irrigate the joint cavity to remove debris. The incision was carefully closed as was done in sham group. For murine model of costal cartilage graft, allogenic costal cartilage grafts were harvested from cartilaginous part of fifth to sixth ribs of 8-week-old male C57BL/6J mice. Perichondrium was carefully removed by microscopic tweezers and costal cartilage fragments ready for use were kept in phosphate buffer saline (PBS) on ice. An osteochondral defect was made as described above. A costal cartilage fragment of suitable size was picked out and pressed into the defect, and then trimmed to fit the articular surface. After surgery, all mice were allowed to move freely inside the cages without load restriction.

Gait Analysis

Gait behaviors of mice at 8 weeks after surgery were collected by video-based Catwalk gait analysis system (MobileDatum Co., Ltd), which is composed of an enclosed walkway, a light source, a high-speed camera, and an analysis software. Briefly, each mouse was placed individually in the walkway and allowed to walk freely from one side to the other side after adaptive training. Footprints and walking time were recorded by high-speed camera and gait parameters were analyzed by the Catwalk software. According to previous references, print area, duty cycle, and stride length were adopted as main parameters in this study.[28,29]

Specimen Preparation

Mice were sacrificed under anesthesia at 2, 4, and 8 weeks after surgery. Specimen of costal cartilage and knee joint were collected and then fixed with 4% paraformaldehyde for 24 hours. For HE, SO, and immunohistochemical staining, specimen was decalcified in 10% ethylenediaminetetraacetic acid (EDTA) in 37°C for 2 days and prepared for 6-μm-thick paraffin embedded sagittal sections. For Goldner's trichrome staining, specimen was prepared for 20-μm-thick hard tissue sections. For immunofluorescence staining, specimen was also decalcified in 10% EDTA in 37°C for 2 days and then incubated at 4°C with 15% sucrose for 24 hours and 30% sucrose for another 24 hours. They were placed in optimal cutting temperature (OCT) compound (Sakura) and frozen at −20°C until they were sectioned by cryotome (Leica) to generate 10-μm sections.

3D Optical Profiles and Micro-Computed Tomography Analysis (Micro-CT)

For 3D optical profiling, skin and muscles of knee joint were removed, and the articular surface of distal femur was exposed. 3D optical profiles of articular surface were scanned by 3D optical profiler ZeGage™ Pro (ZYGO) to evaluate the articular cartilage smoothness precisely. Graph describing articular surface quantitively was drawn by Microsoft Excel according to the width and depth provided by the results of 3D optical profiles for 3 different samples from sham, defect and graft group respectively. For micro-CT, knee joints were stored in 70% ethanol after fixed. All samples were scanned at 9 μm resolution by a micro-CT scanner (SkyScan 1176, Kontich). Three-dimensional reconstructed images were visualized using CTVox software (Bruker MicroCT, Kontich). The sagittal images of the knee joints were obtained by DataViewer (Bruker MicroCT, Kontich).

Histology

The paraffin embedded sections of knee joints were stained with hematoxylin–eosin (HE) and safranin O (SO)/fast green. The cellularity and morphology of cartilage and subchondral bone were examined by 2 independent experienced researchers in a blinded manner. The histological assessment of cartilage defect was evaluated by International Cartilage Repair Society (ICRS) scores.[30]

Immunohistochemical Staining

For immunohistochemistry (IHC) staining, sections were treated with citric acid antigen repair solution (Ribiology) in micro-oven, and then treated with 3% H_2O_2 at room temperature for 25 minutes. Nonspecific binding sites was blocked by 10% bovine serum albumin for 30 min at room temperature. The sections were then incubated with the primary antibody (Cell signaling technology) overnight at 4°C. Finally, the sections were incubated with biotinylated secondary antibody (DAKO) and visualized by DAB solution (DAKO) for IHC. The sections were also counterstained with hematoxylin. For Goldner's trichrome staining, the sections were embedded in collodion after deplasticization by 2-methoxyethylacetate. Collodion were fixed by 80% ethanol. Then the sections were stained by iron-hematoxylin for 15 min, acid fuchsin for 15 minutes, Orange G for 5 minutes, and light green for 10 minutes. Xylene was used to remove the collodion.

Immunofluorescence Staining

The frozen sections were treated with 0.1% Triton X-100 for 10 minutes and blocked by 3% bovine serum albumin (BSA) for 1 hour. The sections were incubated with goat anti-CD31 (R&D) in 0.2% BSA at 4°C overnight. Then they were incubated with donkey anti-goat secondary antibody in 0.2% BSA at room temperature for 2 hours followed by phalloidin 647 (Invitrogen, 1:250) in PBS at room
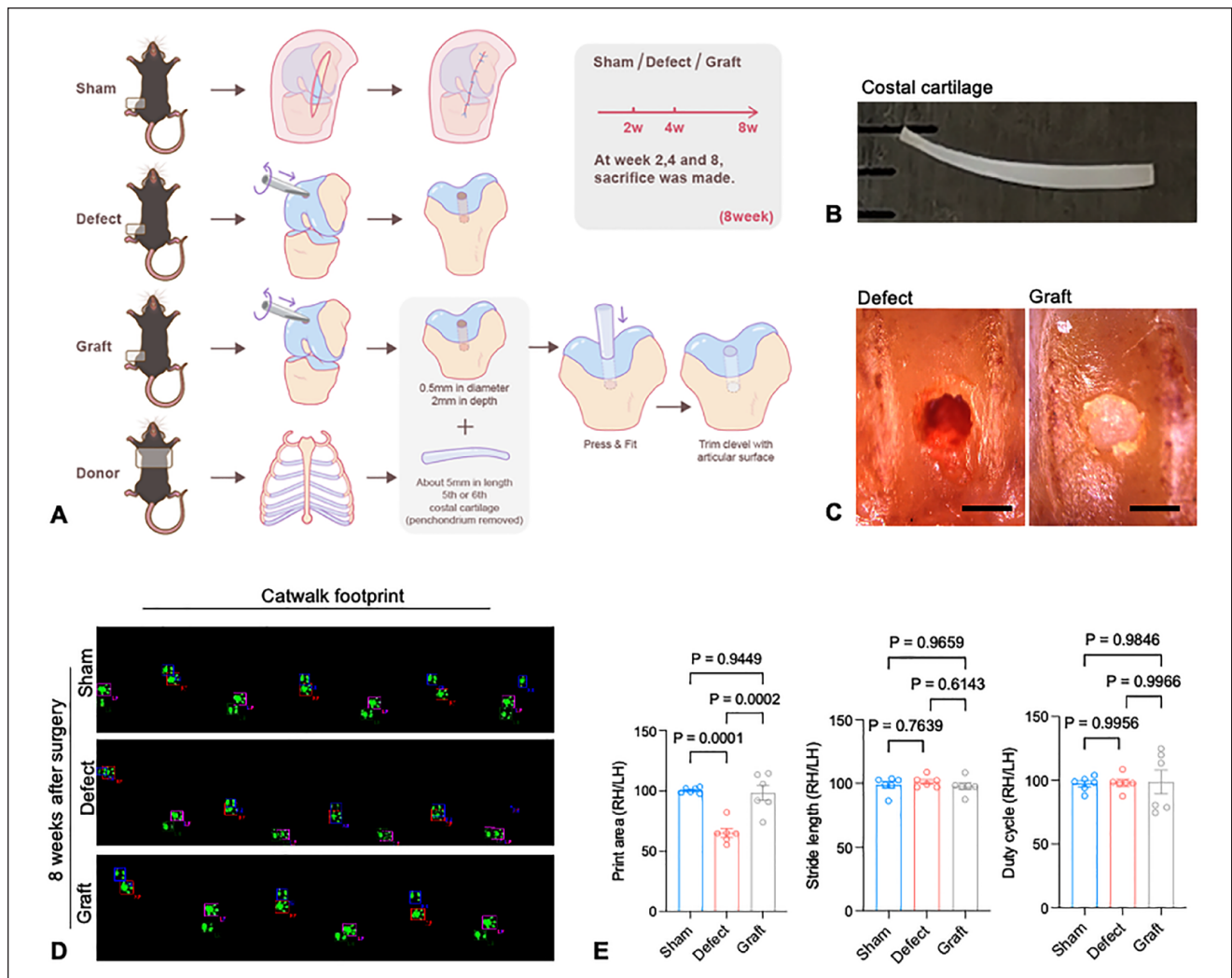
Figure 1. Costal cartilage graft in C57BL/6J mice model. (**A**) Diagram describing experimental groups and surgical procedures for the groups of sham, defect, and graft. A medial para-patellar incision was made for all groups, and osteochondral defects (0.5 mm in diameter and 2 mm in depth) were made in the patellar groove for both defect and graft groups. The costal cartilage from fifth or sixth rib with perichondrium removed were trimmed to fit the osteochondral defect for the graft group. (**B**) Macroscopic picture of fifth costal cartilage with perichondrium removed. (**C**) Intraoperative photographs of mice in defect and graft groups. Scale bar = 500 μm. (**D**) Representative signal images of the Catwalk footprints. (**E**) Gait parameters compared among groups (n = 6 for each group). Values are presented as the ratio of the RH (operated knee)/ LH (contralateral knee). RH = right hind; LH = left hind.

temperature for 1 hour and DAPI (Servicebio) for 10 minutes. The stained tissue sections were observed and imaged by LSM710 microscope (Zeiss). Osteocytes dendrites were recorded by overexposure of phalloidin.

Statistical Analysis

Data were analyzed and presented using GraphPad Prism version 8.0. All results were shown as means ± SEM of independent individuals. Statistical significances were calculated by Student's *t* test for 2 group comparisons and analysis of variance (ANOVA) for multiple group comparisons as indicated in figure legends. *p*-values were considered significant at $p < .05$.

Results

Establish a Costal Cartilage Graft Mouse Model to Repair Articular Osteochondral Defect

Taking advantage of costal cartilage, we designed a costal cartilage graft mouse model to study the endochondral ossification process during the repairment of articular osteochondral defect (**Fig. 1A**). As shown in **Figure 1A**, costal cartilage graft, osteochondral defect, and sham surgery were performed on right hind legs of 8-week-old mice. In defect and cartilage graft group, osteochondral defects (0.5 mm in diameter and 2 mm in depth) were punched by syringe needle in the patellar groove. In
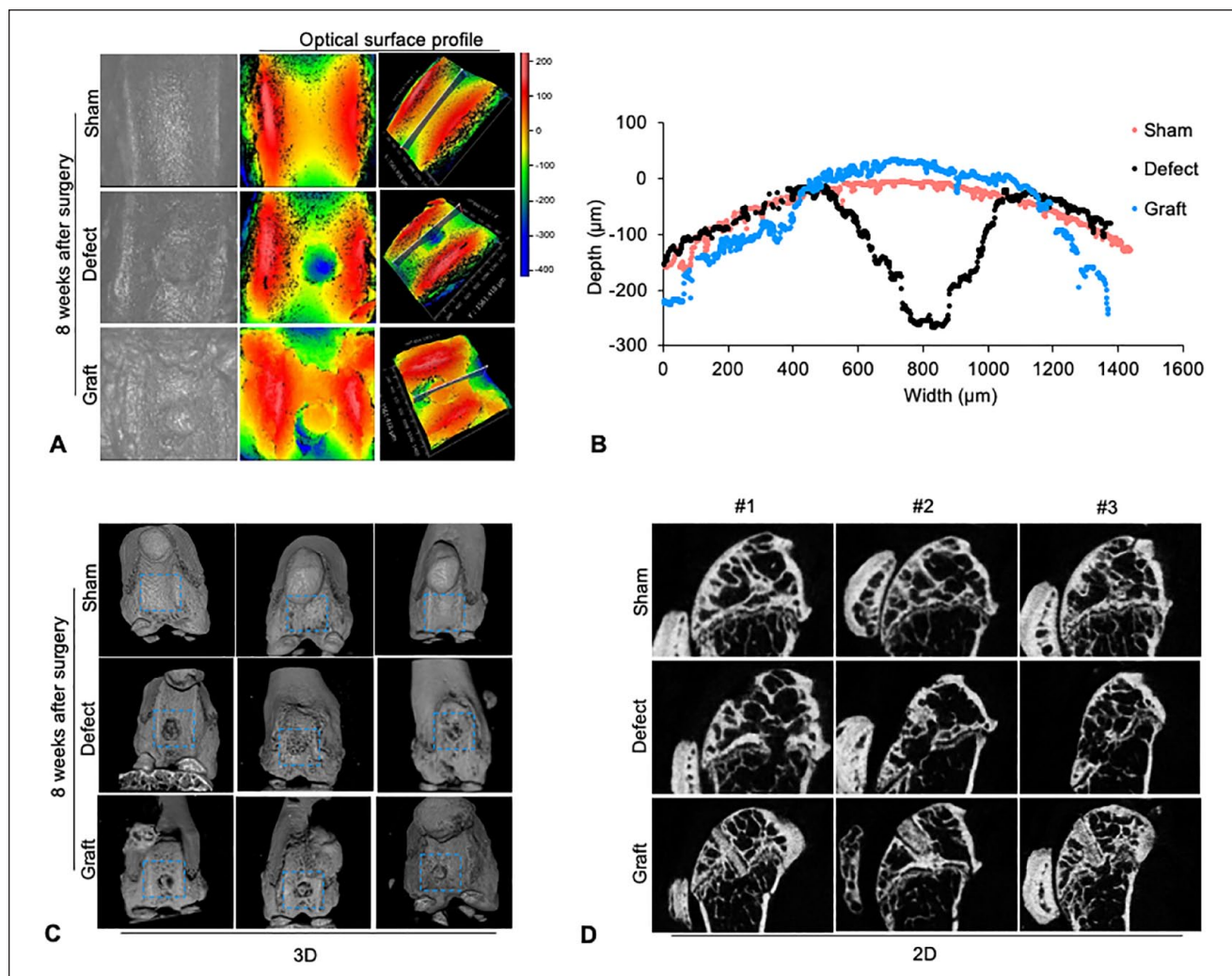
Figure 2. Costal cartilage graft restores both articular cartilage surface and subchondral area. (**A**) 3D optical profiles of representative samples from sham, defect and graft groups. (**B**) Graph depicting relative width and depth of the articular surface at the sagittal planes in **Figure 2A**. (**C**) 3D reconstruction of micro-CT of distal femur. (**D**) 2D sagittal cross-sections of micro-CT. micro-CT = micro-computed tomography.

consideration of fitting the defect appropriately, the costal cartilage from fifth or sixth rib was chosen as graft, and perichondrium of the costal cartilage was carefully removed (**Fig. 1B**). In cartilage graft group, the costal cartilage was pressed into the defect, and then trimmed to fit the articular surface (**Fig. 1C**).

To assess the repair effect of costal cartilage graft on knee joint function, gait analysis was carried out by Catwalk system at 8 weeks after surgery. The defect group showed a decrease in print area compared with sham group, indicating a weightbearing shift from the defected right knee to left knee (**Fig. 1D** and **E**). Such weightbearing imbalance was caused by the disabling of defect knee, most likely the structural changes and full-depth defect as reported.[28,29] The graft group in contrast showed good recovery of joint function, as the print area had no significant difference with the

sham group (**Fig. 1D** and **E**). Although other indicators associated with gait alteration caused by pain were not significantly different between the 3 groups, there were a slight increase in stride length when we compare those of defect group to those of sham group which is alleviated in the graft group (**Fig. 1E**).

Repaired Cartilage Surface and Subchondral Area

To further study repair effect of costal cartilage graft in the defected knee joint, the articular surface of patellar groove was scanned by 3D optical profiles. The articular surface in the graft group remains smooth and continuous at 8 weeks as shown in 3D optical profiles (**Fig. 2A**). Micro-CT was then employed to evaluate the reconstruction

of subchondral structure. The defect group fail to form complete subchondral structure at 8 weeks, a critical bone defect was shown in the patellar grove of distal femur (**Fig. 2C**), and the trabecular structure of defect site was disorganized (**Fig. 2D**). While in the graft group, the shape of distal femur was well preserved (**Fig. 2D**). In detail, the original defect area showed mineralized components fitting with the adjacent bone structure in the surface of subchondral trabecular bone (**Fig. 2D**). The preservation of subchondral area and articular cartilage continuity may be due to the sufficient support offered by tight integration of costal cartilage into host environment.

To explore the nature of repaired cartilage and subchondral bone, histological analysis was performed. At 8 weeks after surgery, HE and SO staining demonstrated that in graft group, cartilage defect was fitted with costal cartilage graft, which show similar quality to articular cartilage (**Fig. 3B**). While in defect group, no cartilage formation at the defect site and only partially bone repair could be observed in cartilage and subchondral area (**Fig. 3A** and **B**), and the adjacent knee cartilage near the defect site showed poorer quality than cartilage adjacent to the graft site in graft group (**Fig. 3B**). Furthermore, normal articular cartilage is embedded by abundant extracellular matrix: type-II collagen. Immunohistochemistry showed that in defect group, no collagen II positive matrix was formed at the defect site, while in graft group, the repair tissue was collagen II positive, indicating that the collagen matrix of repair tissue remains the feature of hyaline cartilage like that of nature articular cartilage (**Fig. 2D**). Moreover, histological scoring of cartilage repair was carried out by The International Cartilage Repair Society (ICRS) score. ICRS score of graft group was significantly higher than that of defect group (**Fig. 3B**), indicating an overall successful histological repair of osteochondral defect by costal cartilage graft.

Formation of Graft-Cartilage and Graft-Bone Interfaces

In addition to overall repair effect, a stable graft-cartilage interface and graft-bone interface gradually formed from 2 weeks to 8 weeks after surgery (**Fig. 3B**). At 2 weeks, there was only fibrous tissue filling the gap between graft and host tissue, while at 8 weeks, those fibrous tissue disappeared (**Fig. 3B**). Instead, graft and articular cartilage fused together, and bone tissue grew into the graft at subchondral area (**Fig. 3B**). Thereby, a biological integration of graft and host took place after transplanted and graft-cartilage and graft-bone interfaces formed, which could not be observed in normal costal cartilage of 8-week-old mice (**Fig. 3C**), indicating those changes occurred under the influence of cartilage and subchondral environment. The formation of biological interfaces might contribute to the stability of cartilage graft and offer support for articular surface.

Intriguingly, at subchondral area in graft group, new osteoid was found between mineralized bone and costal cartilage as transition, which was recognized by Goldner's trichrome staining (**Fig. 3D**), and bone formation could be observed at the margin of the graft and even inside the graft (**Fig. 3D**), which is in consistent with micro-CT results (**Fig. 2D**). To conclude, the costal cartilage graft at the graft-bone interface was partially replaced by bone tissue and bone marrow at 8 weeks. It could be inferred that the costal cartilage graft underwent endochondral ossification after transplanted. Notably, the costal cartilage transplanted with perichondrium lost its viability and showed poor integration into host after 8 weeks (**Fig. 3E**). It indicates that the communication between costal chondrocytes and subchondral environment plays an important part in the formation of biological interface.

Ossification of Costal Cartilage at Graft-Bone Interface

To elucidate the mechanism behind biological interface formation of costal cartilage graft, mGmT transgenic mice were used as donor of costal cartilage to trace the fate of costal chondrocytes in graft. At 8 weeks after surgery, confocal imaging on serial sections observed maintained nuclei integrity in most of the chondrocytes, indicating most cells from graft were survived (**Fig. 4B**), which may play an important part in the formation of interface. The graft-cartilage interface remained abundant live cells in both graft and host cartilage, and no other cell types can be observed in between (**Fig. 4B** and **C**), indicating a good integration of graft costal chondrocyte and host cartilage chondrocyte, consistent with the histological findings (**Figs. 3B** and **4B**).

At the graft-bone interface, like histology results, fluorescence results demonstrated that bone and bone marrow like structures formed surround the graft at subchondral area (**Fig. 4B** and **Fig. 3C**). In detail, confocal imaging showed denser chondrocytes distribution at margin of costal cartilage before transplantation (**Fig. 4A**). However, at 8 weeks, those cells with high density before graft disappeared into cell debris, which were closely wrapped by the osteocytes from host (**Fig. 4D**). Intriguingly, in some other regions, osteocytes with evident fluorescence were observed (**Fig. 4E**). Since osteocytes were not present in normal costal cartilage before graft (**Fig. 4A**), and graft-cartilage interfaces (**Fig. 4C**), it can be inferred that numbers of donor-derived costal chondrocytes turned into osteocytes under the influence of subchondral environment. The 2 types of interface development are consistent with current hypothesis of endochondral ossification. Moreover, new bone formation at the interface is accompanied by ingrowth of CD31 positive blood vessels (**Fig. 5A**). Those blood vessels were located between graft cartilage and newly formed osteocytes (**Fig. 5B**). Accumulating evidence showed that
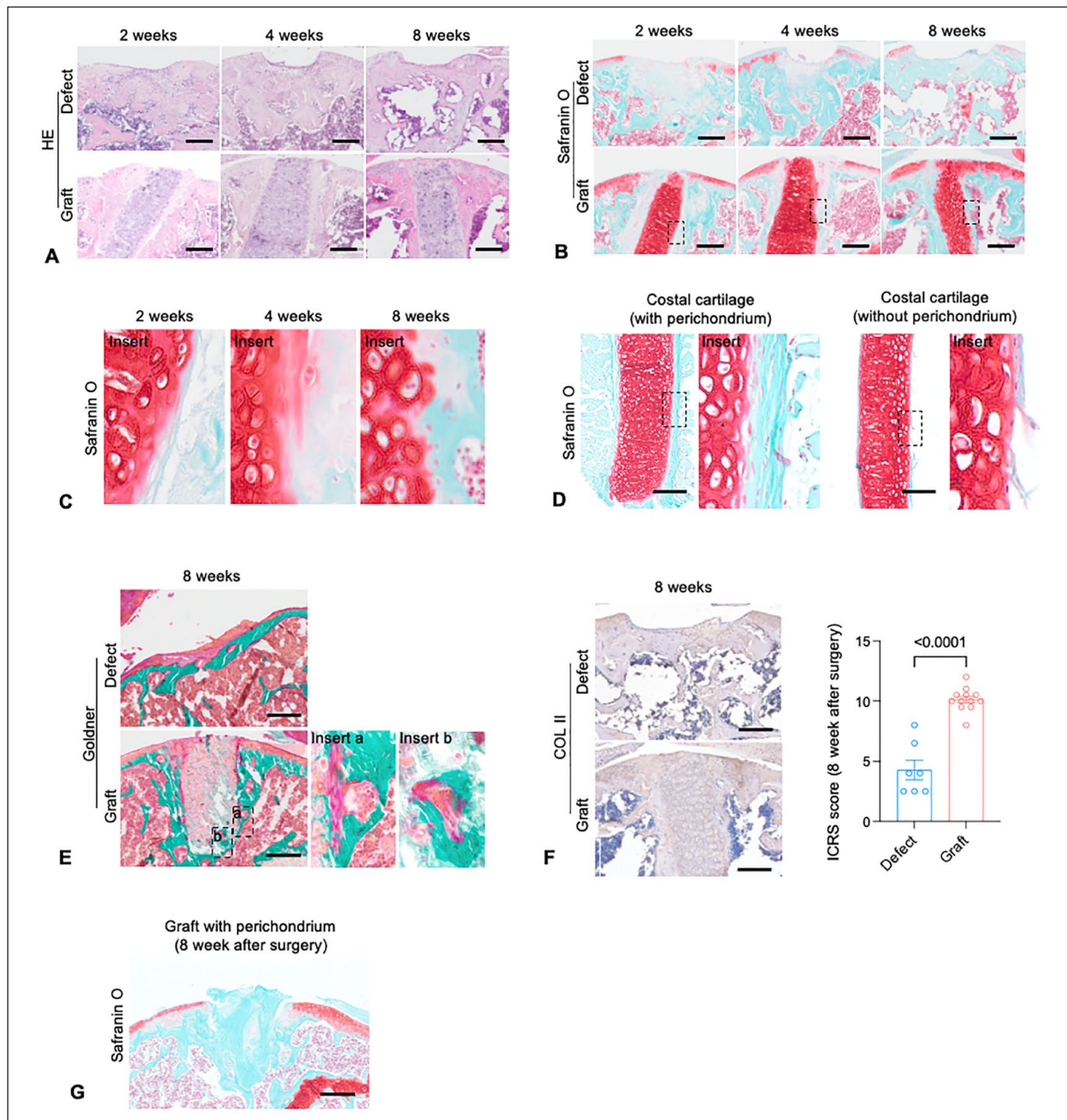
Figure 3. Formation of graft-cartilage and graft-bone interfaces in costal cartilage graft model. (**A**) Hematoxylin and eosin-stained sections of distal femurs from mice in defect and graft groups at 2, 4, 8 weeks after surgery. (**B**) Safranin O/fast green stained sections of distal femurs from mice in defect and graft group at 2, 4, 8 weeks after surgery and ICRS scores to indicate the overall histological repair of osteochondral defect. (**C**) Magnification of graft-bone interface in (**B**). (**D**) Safranin O/fast green stained sections of costal cartilage from 8-week-age C57BL/6J mice. (**E**) Goldner's trichrome stained sections of distal femurs from mice in defect and graft groups at 8 weeks after surgery. (**F**) Immunohistochemical staining of Collagen II and ICRS scores in distal femurs from mice in defect and graft groups at 8 weeks after surgery (defect group, n=7; graft group, $n = 12$). (**G**) Safranin O/fast green stained sections of distal femurs from mice that received costal cartilage graft with perichondrium. Scale bar = 200 μm. HE = hematoxylin–eosin; COL II = Collagen II; ICRS = International Cartilage Repair Society.
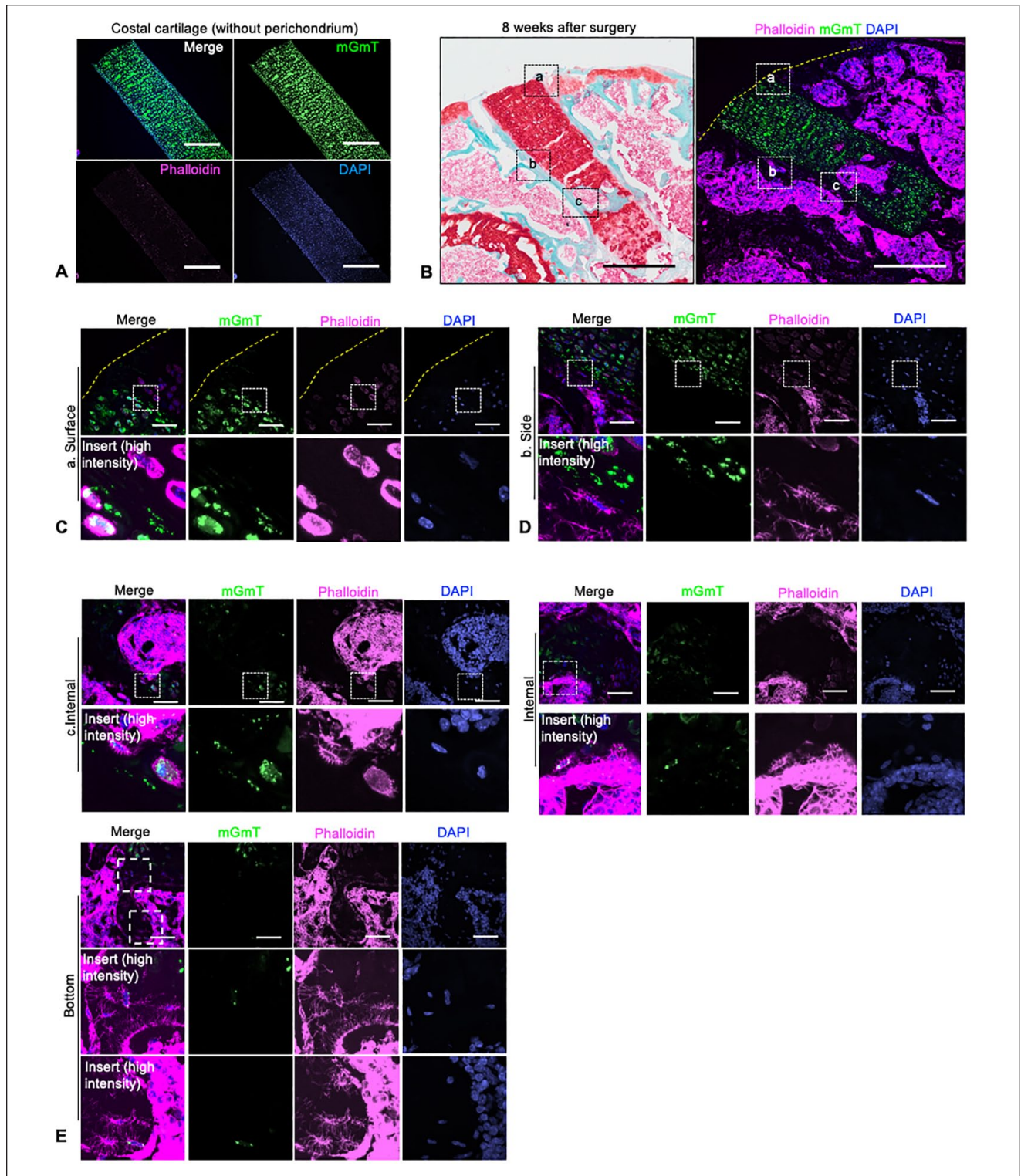
Figure 4. Chondrocytes in graft costal turn into osteocytes at graft-bone interface, but not in graft-cartilage interface. (**A**) Confocal image of costal cartilage without perichondrium from 8-week-age mGmT mice. Scale bar = 100 μm. (**B**) Confocal image of distal femurs from wild-type C57BL/6J mice that received the graft from mGmT mice, and its serial sections stained with Safranin O/fast green. Area outlined in white represents interface in different region: a. graft-cartilage interface at the articular surface; b. graft-bone interface at the side of the graft; c. graft-bone interface inside the graft. Scale bar = 100 μm. (**C**) Magnification of interfaces of a. in **Figure 4B**. Insert shows the chondrocytes from graft and host. Scale bar = 25 μm. (**D**) Magnification of interfaces of b. in **Figure 4B**. Insert shows the cellular debris from costal cartilage and osteocytes from host. Three representative confocal images, including b. in **Figure 4B**, of chondrocytes in graft costal that turned into osteocytes at graft-bone interface. Scale bar = 25 μm. (**E**) Magnification of the interface of c. in **Figure 4B** and interfaces from 2 other mice as biological repeats. Scale bar = 25 μm. mGmT = membrane-targeted green fluorescent protein and membrane-targeted tandem dimer Tomato. DAPI = 4′,6-diamidino-2-phenylindole.
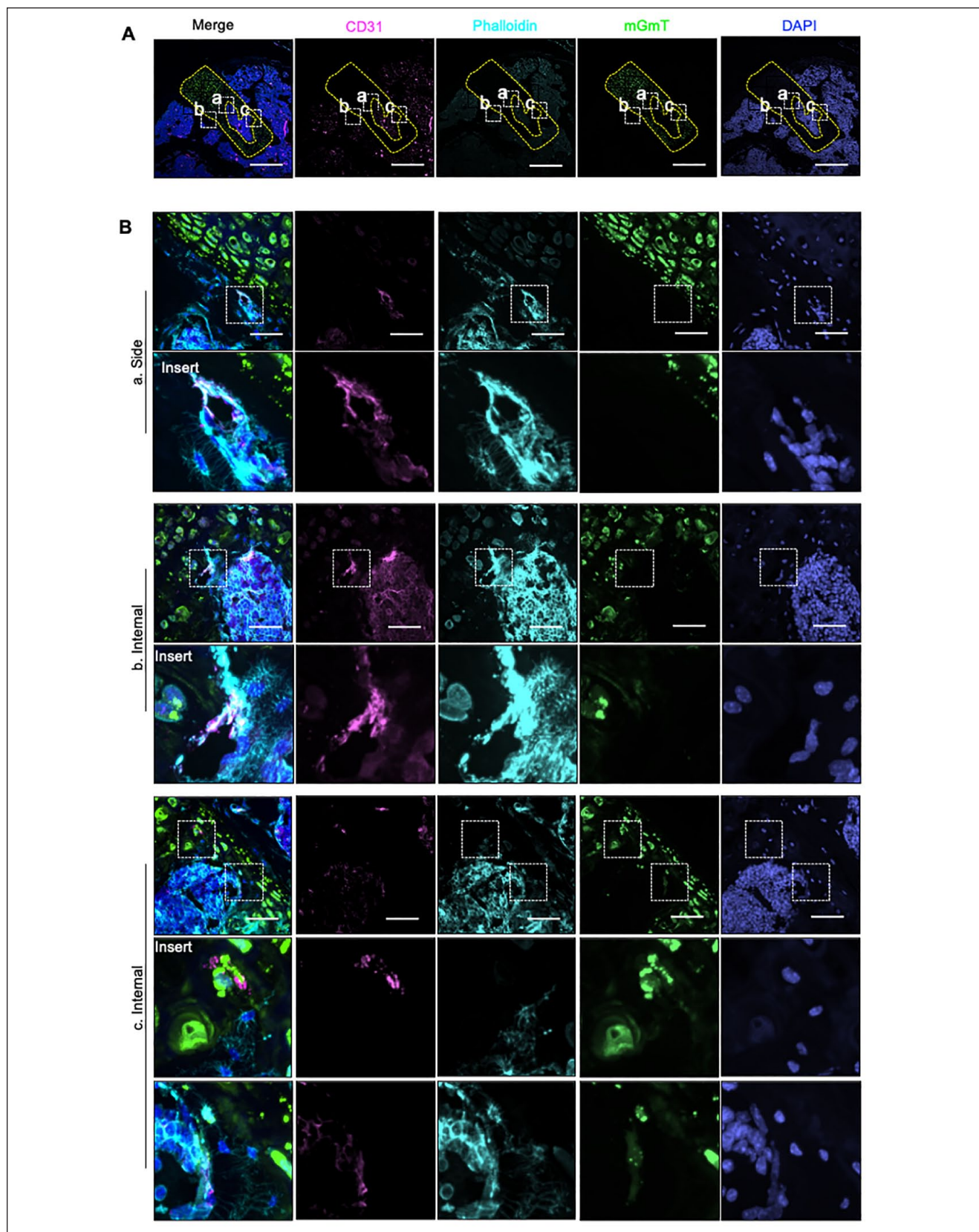
Figure 5. Blood vessels at the graft-bone interface mediate the ossification of costal cartilage graft. (**A**) Confocal image of distal femurs from wild-type C57BL/6J mice that received the graft from mGmT mice. CD31 were stained for blood vessels. Area outlined in yellow represents the graft and white represents interface in different region. Scale bar = 100 μm. (**B**) Magnification of the interface in **Figure 5A**. Scale bar = 25 μm. mGmT = membrane-targeted green fluorescent protein and membrane-targeted tandem dimer Tomato. DAPI = 4',6-diamidino-2-phenylindole.

the growth of blood vessels in bone are coupled with osteogenesis.[21] The development of blood vessels along and into the costal cartilage graft further verified the ossification process at the graft-bone interface.

Discussion

Osteochondral defect left untreated leads to pain and disability of patients and has placed heavy economic burden on society. The compositional similarity of articular cartilage and costal cartilage as well as the hypertrophic nature of costal cartilage make costal cartilage an ideal alternative for osteochondral repair and studying the late differentiation of chondrocytes under different conditions.[11,31] Thus, we proposed a costal cartilage transplantation model, in which hypertrophic costal cartilage graft is transplanted into osteochondral defect in mice knee (**Fig. 1A-C**). This model shows overall repair effect on osteochondral defect as shown by gait analysis (**Fig. 1D** and **E**). The graft incorporates into host and undergoes remodeling to form graft-bone and graft-cartilage interface at 8 weeks after transplantation (**Figs. 2** and **3**). The graft–bone interface exhibits histological traits like physiological transition between articular cartilage and subchondral bone, indicating the successful mimics of this biological process (**Figs. 3** and **4**). The invasion of blood vessels within graft-bone interface indicated the formation of functional bone (**Fig. 5**). It has been reported that hypertrophic chondrocytes and osteoblasts modulate the ingrowth of blood vessels during endochondral ossification by producing vascular endothelial growth factor (VEGF).[32] The blood vessels foster the further development of bone structure.[33]

The malleable nature of costal cartilage made it a 1-step repair strategy for the multi-layered osteochondral complex. On one hand, the endochondral ossification highly relies on the intrusion of vascular structure, which was enriched in subchondral area.[32-34] In the subchondral bone, we observed costal cartilage penetrated by vessels (**Fig. 5**). However, the articular cartilage is of avascular nature,[2,6] which isolated the vessels from costal cartilage at the articular surface (**Fig. 5A**). On the other hand, our previous published study indicated that synovium-derived stromal cells could promotes cartilage repair through their anti-hypertrophic effect of on costal chondrocytes.[35] The surrounding synovial environment could possibly explain why the costal cartilage close to the articular surface wasn't calcified in our model.

Our study on transdifferentiation of hypertrophic chondrocytes during osteochondral repair besides endochondral ossification during development provides insight for clinical treatment. Establishing a stable interface between graft and host has long been a problem for osteochondral repair.[8,36] The osteogenic potential of hypertrophic chondrocytes makes it a good candidate for osteochondral repair

since our study show the changes of the graft are subject to its environment. The graft undergoes endochondral ossification under the influence of subchondral area, so that the graft could integrate into subchondral area and form a biological interface, while the graft near articular surface doesn't lose its cartilage nature, which is appropriate for cartilage repair.

Further, the establishment of mouse cartilage transplant model enables us to take advantage of transgenic mice for characterizing the molecular mechanisms of endochondral ossification in osteochondral repair. Numerous studies have reported the molecular mechanisms of chondrocyte maturation and hypertrophy.[37-40] But only recently a few studies focus on the intrinsic mechanisms of transdifferentiation of hypertrophic chondrocytes into osteocytes.[41,42] The molecular basis and driving force of osteogenic transdifferentiation have not been fully elucidated yet. Intriguingly, among those studies, diabetic pregnancy of mice can interfere with the chondrocytes transdifferentiation through NF-κB signaling in the situation of embryonic long-bone development,[42] which indicates that metabolic environment might play a role. Based on our findings, the presence of subchondral area including trabecular bone, bone marrow cells and vasculature but not articular cartilage induce the transdifferentiation of hypertrophic chondrocytes to osteocytes *in vivo*.

This study has several limitations. First, many factors affect osteochondral repair, such as age, sex, and degree or location of osteochondral defect, our study only investigate adult male animals of 8-week-old and the osteochondral defect of non-weightbearing area. Although 8-week-old mice were widely used as adult mice to study cartilage repair,[17-23] mice over 3-month-old is generally considered skeletally mature in previous study.[43-45] 8-week-old mice haven't achieved peak bone parameters such as bone density and bone strength, which might affect the repair effect. Further study will be conducted on skeletally mature mice to verify our conclusion. Secondly, since the costal cartilage have the potential of endochondral ossification, a longer period than 8 weeks postsurgery might be needed for observation of repair effect and outcome of the graft. Further study with longer observation will be conducted to explore the mechanism determining the differentiation of costal cartilage. Moreover, we used mice as the animal model. As the walking load differs between human legs and mice hind limb, the process of osteochondral repair may be different from that in humans.

In conclusion, costal cartilage grafting shows both functional and histological repair of osteochondral defect in mice. Graft-derived costal chondrocytes differentiate into osteocytes and contribute to endochondral ossification. Our findings support the idea that costal cartilage graft as feasible treatment for osteochondral defect and show how cartilaginous graft dynamically adapt to local environment and

add to the knowledge of the mechanisms underlying osteochondral repair and graft-host interaction.

Declaration of Conflicting Interests

The author(s) declared no potential conflicts of interest with respect to the research, authorship, and/or publication of this article.

Ethical Statement

All animal experiments were conducted according to the regulations and with approval of the Animal Care and Use Committee of Shanghai Sixth People's Hospital.

ORCID iDs

Yiyang Ma https://orcid.org/0000-0002-6218-8593
Kaiwen Zheng https://orcid.org/0000-0003-3184-5375
Changqing Zhang https://orcid.org/0000-0002-7408-4126

References

1. Armiento AR, Alini M, Stoddart MJ. Articular fibrocartilage–why does hyaline cartilage fail to repair? Adv Drug Deliv Rev. 2019;146:289-305. doi:10.1016/j.addr.2018.12.015.

2. Johnstone B, Alini M, Cucchiarini M, Dodge GR, Eglin D, Guilak F, et al. Tissue engineering for articular cartilage repair–the state of the art. Eur Cell Mater. 2013;25:248-67. doi:10.22203/ecm.v025a18.

3. Heir S, Nerhus TK, Rotterud JH, Loken S, Ekeland A, Engebretsen L, et al. Focal cartilage defects in the knee impair quality of life as much as severe osteoarthritis a comparison of knee injury and osteoarthritis outcome score in 4 patient categories scheduled for knee surgery. Am J Sports Med. 2010;38(2):231-7. doi:10.1177/0363546509352157.

4. Lories RJ, Luyten FP. The bone-cartilage unit in osteoarthritis. Nat Rev Rheumatol. 2011;7(1):43-9. doi:10.1038/nrrheum.2010.197.

5. Makris EA, Gomoll AH, Malizos KN, Hu JC, Athanasiou KA. Repair and tissue engineering techniques for articular cartilage. Nat Rev Rheumatol. 2015;11(1):21-34. doi:10.1038/nrrheum.2014.157.

6. Wei W, Dai H. Articular cartilage and osteochondral tissue engineering techniques: recent advances and challenges. Bioact Mater. 2021;6(12):4830-55. doi:10.1016/j.bioactmat.2021.05.011.

7. Mollon B, Kandel R, Chahal J, Theodoropoulos J. The clinical status of cartilage tissue regeneration in humans. Osteoarthritis Cartilage. 2013;21(12):1824-33. doi:10.1016/j.joca.2013.08.024.

8. Pabbruwe MB, Esfandiari E, Kafienah W, Tarlton JF, Hollander AP. Induction of cartilage integration by a chondrocyte/collagen-scaffold implant. Biomaterials. 2009;30(26):4277-86. doi:10.1016/j.biomaterials.2009.02.052.

9. Donahue RP, Nordberg RC, Bielajew BJ, Hu JC, Athanasiou KA. The effect of neonatal, juvenile, and adult donors on rejuvenated neocartilage functional properties. Tissue Eng Part A. 2022;28(9-10):383-93. doi:10.1089/ten.TEA.2021.0167.

10. Yoon KH, Park JY, Lee JY, Lee E, Lee J, Kim SG. Costal chondrocyte-derived pellet-type autologous chondrocyte implantation for treatment of articular cartilage defect. Am J Sports Med. 2020;48(5):1236-45. doi:10.1177/0363546520905565.

11. Huwe LW, Brown WE, Hu JC, Athanasiou KA. Characterization of costal cartilage and its suitability as a cell source for articular cartilage tissue engineering. J Tissue Eng Regen Med. 2018;12(5):1163-76. doi:10.1002/term.2630.

12. Lee J, Lee E, Kim HY, Son Y. Comparison of articular cartilage with costal cartilage in initial cell yield, degree of dedifferentiation during expansion and redifferentiation capacity. Biotechnol Appl Biochem. 2007;48(pt 3):149-58. doi:10.1042/BA20060233.

13. Zhang CQ, Du DJ, Hsu PC, Song YY, Gao Y, Zhu ZZ, et al. Autologous costal cartilage grafting for a large osteochondral lesion of the femoral head: a 1-year single-arm study with 2 additional years of follow-up. J Bone Joint Surg Am. 2022;104(23):2108-16. doi:10.2106/JBJS.22.00542.

14. Bahrami S, Plate U, Dreier R, DuChesne A, Willital GH, Bruckner P. Endochondral ossification of costal cartilage is arrested after chondrocytes have reached hypertrophic stage of late differentiation. Matrix Biol. 2001;19(8):707-15. doi:10.1016/s0945-053x(00)00125-6.

15. Kampen WU, Claassen H, Kirsch T. Mineralization and osteogenesis in the human first rib cartilage. Ann Anat. 1995;177(2):171-7. doi:10.1016/s0940-9602(11)80069-5.

16. Rejtarova O, Hejna P, Soukup T, Kuchar M. Age and sexually dimorphic changes in costal cartilages. A preliminary microscopic study. Forensic Sci Int. 2009;193(1-3):72-8. doi:10.1016/j.forsciint.2009.09.009.

17. Eldridge SE, Barawi A, Wang H, Roelofs AJ, Kaneva M, Guan Z, et al. Agrin induces long-term osteochondral regeneration by supporting repair morphogenesis. Sci Transl Med. 2020;12(559):eaax9086. doi:10.1126/scitranslmed.aax9086.

18. Fitzgerald J, Rich C, Burkhardt D, Allen J, Herzka AS, Little CB. Evidence for articular cartilage regeneration in MRL/MpJ mice. Osteoarthritis Cartilage. 2008;16(11):1319-26. doi:10.1016/j.joca.2008.03.014.

19. Thomas BL, Eldridge SE, Nosrati B, Alvarez M, Thorup AS, Nalesso G, et al. WNT3A-loaded exosomes enable cartilage repair. J Extracell Vesicles. 2021;10(7):e12088. doi:10.1002/jev2.12088.

20. Eltawil NM, De Bari C, Achan P, Pitzalis C, Dell'accio F. A novel in vivo murine model of cartilage regeneration. Age and strain-dependent outcome after joint surface injury. Osteoarthritis Cartilage. 2009;17(6):695-704. doi:10.1016/j.joca.2008.11.003.

21. Matsuoka M, Onodera T, Sasazawa F, Momma D, Baba R, Hontani K, et al. An articular cartilage repair model in common C57Bl/6 mice. Tissue Eng Part C Methods. 2015;21(8):767-72. doi:10.1089/ten.TEC.2014.0440.

22. Stanton H, Rogerson FM, East CJ, Golub SB, Lawlor KE, Meeker CT, et al. ADAMTS5 is the major aggre-

canase in mouse cartilage in vivo and in vitro. Nature. 2005;434(7033):648-52. doi:10.1038/nature03417.

23. Little CB, Meeker CT, Golub SB, Lawlor KE, Farmer PJ, Smith SM, *et al*. Blocking aggrecanase cleavage in the aggrecan interglobular domain abrogates cartilage erosion and promotes cartilage repair. J Clin Invest. 2007;117(6):1627-36. doi:10.1172/JCI30765.

24. Haseeb A, Lefebvre V. Isolation of mouse growth plate-growth plates and articular chondrocytes articular chondrocytes for primary cultures. In: Haqqi TM, Lefebvre V, editors. Chondrocytes: methods and protocols. New York: Springer; 2021. p. 39-51.

25. Shen K, Liu X, Qin H, Chai Y, Wang L, Yu B. HA-g-CS implant and moderate-intensity exercise stimulate subchondral bone remodeling and promote repair of osteochondral defects in mice. Int J Med Sci. 2021;18(16):3808-20. doi:10.7150/ijms.63401.

26. Unno H, Hasegawa M, Suzuki Y, Iino T, Imanaka-Yoshida K, Yoshida T, *et al*. Tenascin-C promotes the repair of cartilage defects in mice. J Orthop Sci. 2020;25(2):324-30. doi:10.1016/j.jos.2019.03.013.

27. Hayashi S, Nakasa T, Ishikawa M, Nakamae A, Miyaki S, Adachi N. Histological Evaluation of early-phase changes in the osteochondral unit after microfracture in a full-thickness cartilage defect rat model. Am J Sports Med. 2018;46(12):3032-9. doi:10.1177/0363546518787287.

28. Ruan MZ, Patel RM, Dawson BC, Jiang MM, Lee BH. Pain, motor and gait assessment of murine osteoarthritis in a cruciate ligament transection model. Osteoarthritis Cartilage. 2013;21(9):1355-64. doi:10.1016/j.joca.2013.06.016

29. Wang Y, Yuan X, Yu K, Meng H, Zheng Y, Peng J, *et al*. Fabrication of nanofibrous microcarriers mimicking extracellular matrix for functional microtissue formation and cartilage regeneration. Biomaterials. 2018;171:118-32. doi:10.1016/j.biomaterials.2018.04.033.

30. Mainil-Varlet P, Aigner T, Brittberg M, Bullough P, Hollander A, Hunziker E, *et al*. Histological assessment of cartilage repair: a report by the Histology Endpoint Committee of the International Cartilage Repair Society (ICRS). J Bone Joint Surg Am. 2003;85(suppl 2):45-57.

31. Srour MK, Fogel JL, Yamaguchi KT, Montgomery AP, Izuhara AK, Misakian AL, *et al*. Natural large-scale regeneration of rib cartilage in a mouse model. J Bone Miner Res. 2015;30(2):297-308. doi:10.1002/jbmr.2326.

32. Sivaraj KK, Adams RH. Blood vessel formation and function in bone. Development. 2016;143(15):2706-15. doi:10.1242/dev.136861.

33. Tuckermann J, Adams RH. The endothelium-bone axis in development, homeostasis and bone and joint disease. Nat Rev Rheumatol. 2021;17(10):608-20. doi:10.1038/s41584-021-00682-3.

34. Eshkar-Oren I, Viukov SV, Salameh S, Krief S, Oh CD, Akiyama H, *et al*. The forming limb skeleton serves as a signaling center for limb vasculature patterning via regulation of Vegf. Development. 2009;136(8):1263-72. doi:10.1242/dev.034199.

35. Ma Y, Zheng K, Pang Y, Xiang F, Gao J, Zhang C, *et al*. Anti-hypertrophic effect of synovium-derived stromal cells on costal chondrocytes promotes cartilage repairs. J Orthop Translat. 2022;32:59-68. doi:10.1016/j.jot.2021.05.002.

36. Agarwal R, Garcia AJ. Biomaterial strategies for engineering implants for enhanced osseointegration and bone repair. Adv Drug Deliv Rev. 2015;94:53-62. doi:10.1016/j.addr.2015.03.013.

37. Stegen S, Laperre K, Eelen G, Rinaldi G, Fraisl P, Torrekens S, *et al*. HIF-1alpha metabolically controls collagen synthesis and modification in chondrocytes. Nature. 2019;565(7740):511-5. doi:10.1038/s41586-019-0874-3.

38. Hirota K, Hirashima T, Horikawa K, Yasoda A, Matsuda M. C-type natriuretic peptide-induced PKA activation promotes endochondral bone formation in hypertrophic chondrocytes. Endocrinology. 2022;163(3):bqac005. doi:10.1210/endocr/bqac005.

39. Chen L, Chen Y, Xu Y, Shen SG, Dai J. Effect of swell1 on regulating chondrocyte hypertrophy during the condylar osteochondral development process in mice. Biochem Biophys Res Commun. 2022;590:42-8. doi:10.1016/j.bbrc.2021.12.086.

40. van Gastel N, Stegen S, Eelen G, Schoors S, Carlier A, Daniels VW, *et al*. Lipid availability determines fate of skeletal progenitor cells via SOX9. Nature. 2020;579(7797):111-7. doi:10.1038/s41586-020-2050-1.

41. Steppe L, Bulow J, Tuckermann J, Ignatius A, Haffner-Luntzer M. Bone mass and osteoblast activity are sex-dependent in mice lacking the estrogen receptor alpha in chondrocytes and osteoblast progenitor cells. Int J Mol Sci. 2022;23(5):2902. doi:10.3390/ijms23052902.

42. Liu X, Qian F, Fan Q, Lin L, He M, Li P, *et al*. NF-kappaB activation impedes the transdifferentiation of hypertrophic chondrocytes at the growth plate of mouse embryos in diabetic pregnancy. J Orthop Translat. 2021;31:52-61. doi:10.1016/j.jot.2021.10.009.

43. Somerville JM, Aspden RM, Armour KE, Armour KJ, Reid DM. Growth of C57BL/6 mice and the material and mechanical properties of cortical bone from the tibia. Calcif Tissue Int. 2004;74(5):469-75. doi:10.1007/s00223-003-0101-x.

44. Ferguson VL, Ayers RA, Bateman TA, Simske SJ. Bone development and age-related bone loss in male C57BL/6J mice. Bone. 2003;33(3):387-98. doi:10.1016/s8756-3282(03)00199-6.

45. Maupin KA, Childress P, Brinker A, Khan F, Abeysekera I, Aguilar IN, *et al*. Skeletal adaptations in young male mice after 4 weeks aboard the International Space Station. npj Microgravity. 2019;5:21. doi:10.1038/s41526-019-0081-4.